

Efficient electron heating by laser in finite sized plasma micro-globular targets by repeated collisions of surface and bulk waves

Animesh Sharma* and Amita Das†

*Department of Physics, Indian Institute of Technology Delhi,
Hauz Khas, New Delhi-110016, India*

G. Ravindra Kumar

*Tata Institute of Fundamental Research
Colaba, Mumbai*

(Dated: December 17, 2024)

A new mechanism of enhanced laser energy absorption in plasma microglobules is demonstrated with the help of two-dimensional Particle-In-Cell (PIC) simulations. The mechanism relies on the excitation of surface and bulk waves and the occurrence of repeated collisions in the confines of the finite-sized microglobular target. The episodic increase in the average particle energy correlates with the repeated collision of the surface and bulk waves that get excited by the laser on the target. It is shown that the size of the microglobular target governs the efficiency of absorption and the timings of episodic events of energy enhancement. This study thereby illustrates the novel efficient possibility that a closed plasma target provides for energy extraction. Parallels of such colliding waves creating havoc in terms of wave breaking etc. can be witnessed on the ocean surface, seismic disturbances traversing as body waves traverse reflecting and refracting in the interior of the Earth along with surface waves (propagating on the curved surface of the Earth) converge at the antipode to create destruction. Our studies here show the importance of choosing closed targets which aid in the process of repeated energy transfer to particles and often their thermalization. The waves keep propagating in the closed confines rather than getting dissipated over an extended region as would happen for extended targets.

I. INTRODUCTION

The question of irreversible energy transfer from the laser Electromagnetic field (EM) to plasma particles has intrigued researchers for a long time. Collisional processes, resonance mechanisms, and conversion to electrostatic waves which subsequently transfer energy to particles via wave breaking and/or phase mixing, have often been invoked for this purpose [1–7]. There have also been attempts to devise ways and means to enhance energy absorption, seek localized absorption, and/or transfer energy predominantly to specific plasma species, etc. [8–23] In this work, we illustrate a novel mechanism that is operative in the context of small finite-sized plasmas which we term here as plasma micro-globules. A 2-D Particle-In-Cell (PIC) simulation has been carried out for this purpose which shows that the colliding surface and bulk waves triggered by laser, easily succumb to wave breaking and efficiently transfer energy to the particles. It should be noted that such a scenario of colliding waves leading to catastrophe is prevalent in a number of contexts. For instance, ocean waves crash on the shore and the returning reflected remnant wave thereafter collides with the next incoming wave. Whenever such a collision happens at an appropriate phase, wave breaking occurs generating huge white water and foams. Another exam-

ple is that of the bulk and surface waves triggered by earthquake which traverse the earth from different paths and converge at antipodes where they may create havoc. In this study we show that similar processes in plasma micro-globular targets facilitate efficient energy transfer in comparison to conventional planar targets.

This paper is organised as follows. In Section II, we describe the simulation set-up. Section III contains diagnostics and analysis that illustrate the novel aspect associated with the globular plasma target leading to enhanced energy absorption. In Section IV we summarize and conclude.

II. SIMULATION DETAILS

A 2D Particle-In-Cell (PIC) simulations have been carried out to illustrate a novel mechanism that is operative in the context of the interaction of laser with a finite-size plasma micro-globule. A fully relativistic, massively-parallel PIC code EPOCH [21] has been used for this purpose. The 2D schematic of the X-Y plane has been depicted in Fig.1. The simulation box is $100\mu\text{m} \times 100\mu\text{m}$ with 12000×12000 cells and the grid size is $dx = dy = 0.00833\mu\text{m}$. A fully ionized electron-ion plasma in the shape of a circular microglobule has been placed inside the simulation box as shown in Fig.1. A laser pulse propagating along the x axis is incident normal to this plasma globule. The ion-electron mass ratio has been taken as 1836. Other details about the simula-

* animesh.sharma.research@gmail.com

† amitadas3@yahoo.com

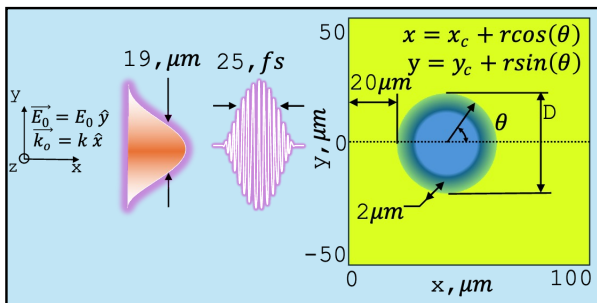


Figure 1. The figure illustrates a schematic drawing of the simulation box. The light green box inside the figure indicates the simulation domain. The laser pulse polarized along \hat{y} is incident from the left side.

tion parameters have been shown in Table I. We have considered three distinct values of the diameter of the plasma globular target in our studies, namely $15\mu m$, $30\mu m$, and $60\mu m$. In addition we have also considered the case of a planar target for comparison. The microglobular target has a density gradient extending $2\mu m$ from its boundary towards the interior. The case of a sharp density profile has also been considered. The density in the interior is constant and is about 10 times the critical density of the laser. The laser pulse has a wavelength of $800nm$ and a spot size whose full-width at a half-maximum (FWHM) is $19\mu m$. The pulse duration is about $25fs$. The laser intensity for these studies have been restricted to non-relativistic regime wherein the normalized vector potential has a value of $a_0 = 0.5$. As mentioned earlier, the laser propagates along x direction and hits the vacuum-plasma interface from the left side of the simulation box. The laser is chosen to be plane polarised with its electric field (E_l) along the y axis, as shown in Fig. 1. The boundary conditions are taken as absorbing for fields as well as for particles. The number of particles in each cell is chosen as 8×8 . The dynamics of both electrons and ions have been considered. Preliminary 3-D simulation study has also been carried out which confirm the salient observations and inferences drawn by 2-D studies.

III. OBSERVATIONS

The evolution of the electron kinetic energy (KE) in the target has been shown in Fig.2. The laser hits the plasma target at $t = 66fs$, thereafter the increase in KE can be observed. This figure shows the KE evolution for three different size of the target diameter. The acquired KE is highest for the smallest sized $15\mu m$ target. In fact, for the planar target, there is negligible energy gain even when the simulation is run for a much longer duration. The other characteristic feature of these energy gain plots is the appearance of distinct peaks. For the $15\mu m$ target the timings of the three peaks have been depicted by t_1, t_2 and t_3 respectively. The inset clearly

Table I. Simulation Parameters

Parameters	Standard Units	
Laser		
Wavelength	λ_L	800 nm
Frequency	ω_L	3
Intensity	$a_o = 0.5$	$5.37 \times 10^{17} W/cm^2$
Plasma		
Electron Plasma frequency	ω_{pe}	$7.443 \times 10^{15} rad/s$
Critical density	$n_c(\omega_L)$	$1.74 \times 10^{27} 1/m^3$
Electron number density	n_e	$10n_c, 1.74 \times 10^{28} 1/m^3$
Ion number density	n_i	$1.74 \times 10^{28} 1/m^3$
Mass of electrons	m_e	$9.109 \times 10^{-31} kg$
Mass of ions	m_i	$1836m_e$
Case	Diameter	
A	15	
B	30	
C	60	
D	Slab	

shows that as one increases the diameter of the target the interval between the peaks becomes longer. The appearance of these peaks indicates that around these instances some mechanism is operative which enhances the energy transfer process from fields to particles. This work aims to unravel this and uncover a novel mechanism of enhanced laser energy absorption process. This process is operative only in the context of small finite-sized globular plasma targets which offer a confined region. We depict the spatial distribution of the charge density and the electric field quiver plots for the smallest $15\mu m$ target in Fig.3. Some of these snapshots have been taken at the same time t_1, t_2 and t_3 demarcated by three vertical lines in Fig.2 about which we discussed in the previous paragraph. There are also additional snapshots taken at intervening times. The complete evolution as a movie is available with us. We now focus on the plots of Fig.3 corresponding to the time $t = t_1$. The kinetic energy of electrons increases and forms the first peak of Fig.2. The spatial distribution of electrons shown in Fig. 3, at $t = 124fs$, and around this time clearly shows that the electrons have been extracted by the laser into the vacuum region in the left side of the target. The extraction is maximum at a certain oblique angle $\theta = 113^\circ$ (depicted in Fig.1) forming two bulges in the left surface of the target for $90^\circ < \theta < 270^\circ$. At $\theta = 180^\circ$ there is a dimple in the spatial electron distribution. The electrons cannot be extracted from here as the electric field is tangential to the target surface. This phase, where two lobes of electrons are extracted, depicted in Fig. 3a, occurs while the laser radiation is present and interacting with the left side of the target surface ($90^\circ < \theta < 270^\circ$). The energy absorption in this particular phase is essentially due to the vacuum-like heating process [17]. The laser electric field which is normal at $\theta = 180^\circ$ becomes oblique at other angles due to the curvature of the target. It is for this reason that no such electron extraction occurs

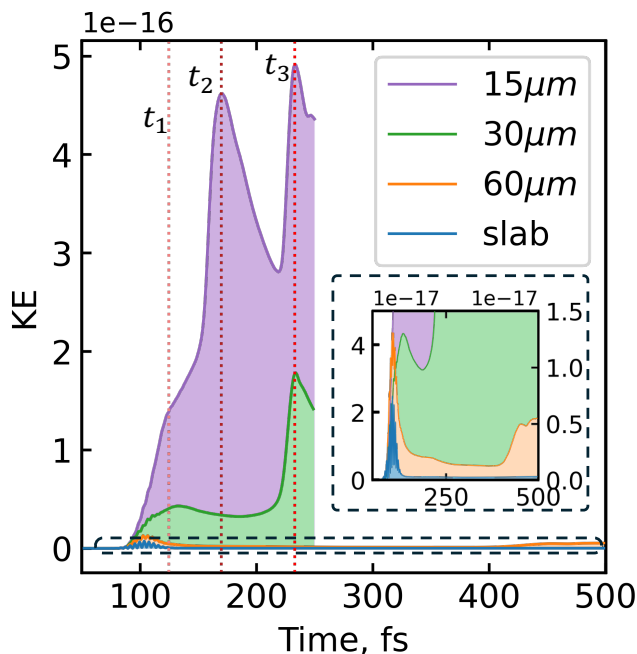


Figure 2. Temporal Evolution of Average Kinetic Energy of Electrons for target diameters of $15\mu m$, $30\mu m$, $60\mu m$ and *slab*. The peaks at t_1 , t_2 and t_3 in $15\mu m$ target correspond to the time of the hump (for ease we call it a first peak) and the appearance of the two peaks respectively. Clearly, at these times some episodic phenomena occurs which facilitates a large transfer of energy.

for planar targets. It is also evident from Fig.2 which shows that the kinetic energy acquired by the electrons for the planar target is negligible. As the laser propagates it impinges upon the target surface with increasing values of $\alpha = |\theta - 180^\circ|$ (from zero to 90°). A surface disturbance of electron density clinging and propagating along the target surface is observed during this phase. After hitting the target at the top (*T*) and bottom (*B*) surfaces at $\alpha = 90^\circ$, the laser simply grazes past the target. The right side of the target is thus not illuminated by the laser. The surface wave of the electron density, on the other hand, propagates along the curvature of the target surface from both top and bottom sides and collides at $\theta = 0^\circ$ when $t = t_2$ corresponding to the appearance of the peak shown in Fig.2. For a target with a bigger diameter this surface wave takes a longer time to arrive and collide at $\theta = 0^\circ$. This explains the increased duration between peaks with increasing diameter of the target. This matches with simple estimates as we now demonstrate. For the $15\mu m$, target the interval between collisions, $(t_2 - t_1) = \Delta t_{15} \sim 48 fs$. For the target with double the diameter of $30\mu m$ this interval is $\Delta t_{30} \sim 101 fs$. We note that the ratio of the two intervals $\Delta t_{15}/\Delta t_{30} \sim 48/101 \approx 2 = 15/30$. This clearly illustrates that as expected the disturbances take proportionately longer time for bigger targets to travel from opposite sides and collide. For the $15\mu m$ target the

time t_3 refers to the time when the disturbance sloshes back and hits the front surface of the target as can be observed from the subplot (f) of Fig.3. The electric field quiver subplots in this figure also show a surface wave propagating back and forth. In addition, there is also a clear evidence of a bulk wave propagating inside the target. This can be observed from the highlighted region in the electric field quiver plots. It is essentially a stochastic electric field that sloshes back and forth [24] in the bulk region and carries energy with itself. The stochastic nature is evident due to the random direction of the electric field in the highlighted region.

The signatures of the surface wave and the bulk wave propagation has been further demonstrated clearly in Fig.4. This figure shows the space-time plot for the electromagnetic field energy (subplot(a)), and the kinetic (subplot(b)) and thermal energy (subplot(c)) acquired by the electrons. The evolution of these has been shown in the $Xvs.t$ and $Yvs.t$ planes. Here t represents the time. In the plane $Xvs.t$ and $Yvs.t$ plots these quantities have been integrated along Y and X respectively. As the thermal energy shows up primarily only near the target region, the space (both the X and Y axis) has been zoomed for a better perspective. The plots represents the data of the target size $15\mu m$. The F(front), R(rear) Top(T), and Bottom(B) of the target location have been demarcated by straight lines in the space-time plots. The time axis has also been demarcated at three locations corresponding to the appearance of the peak in the kinetic energy plot of Fig.2. As the laser falls on the front surface of the target it primarily gets reflected from the overdense plasma. The bright broad horizontal strip in the $Yvs.t$ plot on subplot (a) denotes the incoming and reflected laser. In the $Xvs.t$ plot, the forward propagation in X and the reversal in the X axis clearly shows the reflection of the EM fields along X . A part of the EM field, however, continues to propagate forward in X circumventing the target surface (see subplot(i,j,k,l) of Fig.3. In the $Yvs.t$ plot, this can be seen as two rays propagating along positive and negative Y with time. Furthermore, two more rays of EM wave energy can be observed to graze past the top and bottom surfaces of the target. The plots of kinetic energy and thermal energy in Fig.4(b) and Fig.4(c) clearly provide evidence that kinetic and thermal energy enhancements occur. In fact these enhancements occur predominantly when the laser has already left the simulation box. The timings of the enhancements of these energies are same as the collisions of disturbances at the rear and again at the front surface. In addition in both these energy plots, the enhanced brightness, within the lines denoting the front-rear and top-bottom surface of the target, is an indicator of the bulk disturbance. This bulk wave seems to emanate from the two bulging regions of the front surface of the target and converge at the other side of the target. A careful inspection of the plots of Fig.4 in fact confirms our earlier assertions on episodic increase of particle energy when the surface and bulk waves collide.

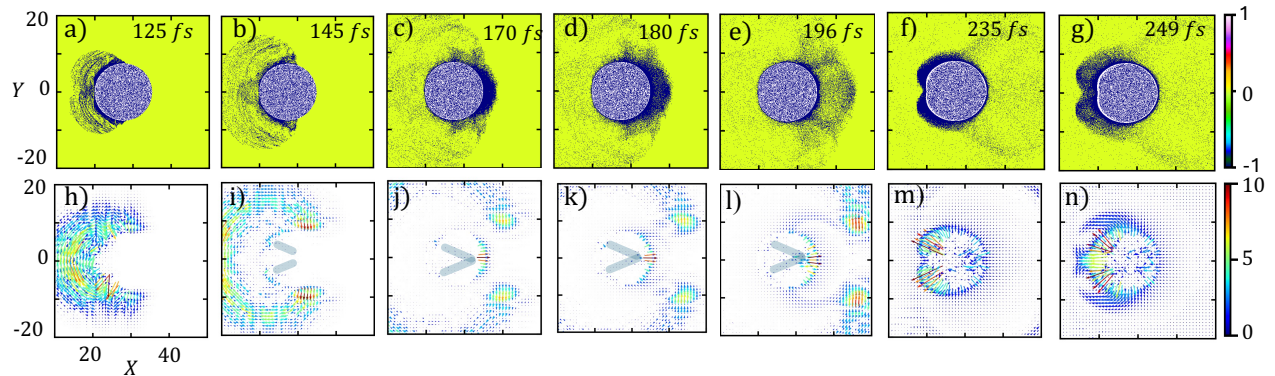


Figure 3. Snapshots of Charge density (a-g) and Electric Field vector (h-i) for $15\mu m$ target. The electrons are blue and ions are white. The electrons are pulled out of the surface in the region where the laser is incident on the target. Disturbances in electron density are seen propagating forward and eventually colliding at subplot(d) when electrons are ejected. The Stochastic bulk waves are seen propagating through the bulk in the quiver plot of the electric field. Enhancements in the field are seen where the surface and bulk disturbances collide

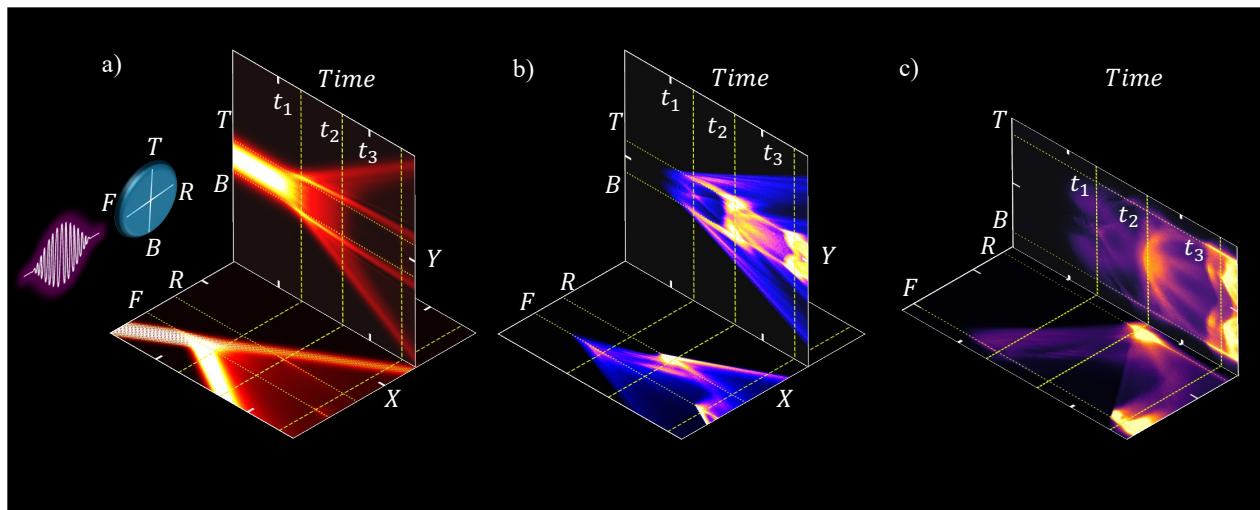


Figure 4. The electromagnetic field energy, kinetic energy of electrons and their thermal energy has been shown in the space time plane in subplot (a), (b) and (c) respectively. The bright colored regions depict higher value of these fields. The letters F,R, T, B denote front, rear, top and bottom position of the target. The reflection of Electromagnetic field energy from F and propagation forward along can be clearly seen in the plot in X vs. t plane in subplot (a). The times stamps t_1, t_2 and t_3 are depicted by straight lines in the time axis. [add color bar]

It should thus be noted that the irreversible energy gain (both kinetic and thermal) by electrons keep happening repeatedly as the disturbances continue to collide alternatively at the front and rear surfaces. This keeps occurring even after the laser has left. The planar slab target does not provide a confined domain for the waves to collide repeatedly. The finite region of the micro-globular targets constrain these waves and offers the opportunity of repeated collisions between them facilitating an irreversible and efficient process of energy transfer.

We have carried out a wide variety of simulations with varying conditions to confirm our conclusions. For instance, we have studied oblique incidence of the laser on

the micro-globules. In this case the disturbances that get generated are asymmetrical. When the two disturbances collide, the one with higher amplitude is seen to drag the smaller one around the surface of the target. The energy transfer process in asymmetric cases get reduced. Furthermore 3-D simulations with spherical targets have also been performed. A typical snapshot has been shown in Fig.5. The surface disturbances and their propagation on the spherical surface is clearly visible in this figure. These waves are observed to converge and lead to an irreversible energy transfer to electrons. Let us also reflect on the suitable micro-globule target size for which this mechanism will be most efficient. We have already demonstrated through the simulation of the var-

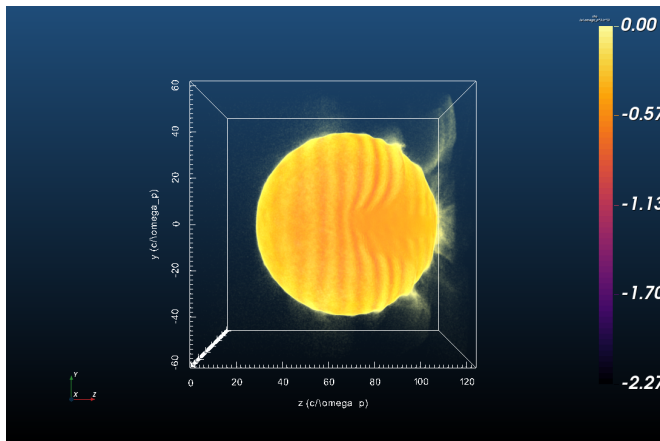


Figure 5. Snapshot of Electron Density of $15\mu\text{m}$ target showing the surface waves and ejection of electrons at rear side of the the target.

ious target sizes that larger the size energy gain is also comparatively smaller. The lower limit of the target size gets decided by the laser wavelength. If the target size is chosen to be smaller than the laser wavelength then the electrons cloud in the entire globule merely oscillate around the ion background as a single entity. Thus the wave like disturbance do not get generated which need to collide/converge to provide efficient irreversible energy transfer episodes.

IV. CONCLUSION

Our studies here show that the the efficiency of laser energy conversion into the kinetic and thermal energy of electrons can be dramatically increased by choosing a micro-globular target. This happens as the finite closed region of the micro-globular target constrains the disturbances and permits their repeated collisions releasing field energy to irreversible particle kinetic energy. Similar occurrence of energy release through colliding disturbances in closed regions has been viewed in the context of earthquake. The surface and body disturbances in this case propagate on the surface of the earth or in the interior and converge at antipodes to wreck havoc there. The message that our work here conveys is that using similar construction one can extract and convert laser energy efficiently into particle kinetic energy.

V. ACKNOWLEDGEMENTS

The authors thank IIT Delhi HPC facility for provide computational resources. AD acknowledges support from the Anusandhan National Research Foundation (ANRF) of the Government of India through core grant CRG/2022/002782 as well as a J C Bose Fellowship grant JCB/2017/000055. GRK thanks the Department of Atomic Energy for long term support of this research and ANRF for a J C Bose Fellowship grant JBR/2020/000039. AS Acknowledges support from Anusandhan National Research Foundation (ANRF) of the Government of India through core grant CRG/2022/002782.

-
- [1] M. J. Everett, A. Lal, D. Gordon, K. Wharton, C. E. Clayton, W. B. Mori, and C. Joshi, *Phys. Rev. Lett.* **74**, 1355 (1995).
- [2] A. Bergmann and P. Mulser, *Phys. Rev. E* **47**, 3585 (1993).
- [3] C. Maity, A. Sarkar, P. K. Shukla, and N. Chakrabarti, *Phys. Rev. Lett.* **110**, 215002 (2013).
- [4] R. M. G. M. Trines, V. V. Goloviznin, L. P. J. Kamp, and T. J. Schep, *Phys. Rev. E* **63**, 026406 (2001).
- [5] T. Katsouleas and W. B. Mori, *Phys. Rev. Lett.* **61**, 90 (1988).
- [6] T. Katsouleas and W. Mori, *Physical review letters* **61**, 90 (1988).
- [7] S. Sengupta, P. Kaw, V. Saxena, A. Sen, and A. Das, *Plasma Physics and Controlled Fusion* **53**, 074014 (2011).
- [8] S. Maity, L. P. Goswami, A. Vashistha, D. Mandal, and A. Das, *Physical Review E* **105**, 055209 (2022).
- [9] R. Juneja, T. Dhalia, L. P. Goswami, S. Maity, D. Mandal, and A. Das, *Plasma Physics and Controlled Fusion* **65**, 095005 (2023).
- [10] A. Vashistha, D. Mandal, A. Kumar, C. Shukla, and A. Das, *New Journal of Physics* **22**, 063023 (2020).
- [11] A. Vashistha, D. Mandal, S. Maity, and A. Das, *Plasma Physics and Controlled Fusion* **65**, 035006 (2023).
- [12] P. Kaw, *Reviews of Modern Plasma Physics* **1**, 1 (2017).
- [13] A. Das, *Reviews of Modern Plasma Physics* **4**, 10 (2020).
- [14] Y. Nishida, N. Sato, and T. Nagasawa, *IEEE transactions on plasma science* **15**, 243 (1987).
- [15] P. Gibbon and E. Förster, *Plasma physics and controlled fusion* **38**, 769 (1996).
- [16] A. Pukhov, Z.-M. Sheng, and J. Meyer-ter Vehn, *Physics of Plasmas* **6**, 2847 (1999).
- [17] F. Brunel, *Physical review letters* **59**, 52 (1987).
- [18] W. Krueer, *The physics of laser plasma interactions* (crc Press, 2019).
- [19] V. L. Ginzburg, W. L. Sadowski, D. Gallik, and S. C. Brown, *Physics Today* **15**, 70 (1962).
- [20] H. Kim, R. Stenzel, and A. Wong, *Physical Review Letters* **33**, 886 (1974).
- [21] T. Arber, K. Bennett, C. Brady, A. Lawrence-Douglas, M. Ramsay, N. J. Sircombe, P. Gillies, R. Evans, H. Schmitz, A. Bell, *et al.*, *Plasma Physics and Controlled Fusion* **57**, 113001 (2015).
- [22] T. Boyd, *Plasma Physics and Controlled Fusion* **28**, 1887 (1986).

- [23] N. Ebrahim, H. Baldis, C. Joshi, and R. Benesch, Physical Review Letters **45**, 1179 (1980).
- [24] S. Puri, Physics of Fluids **9**, 1043 (1966).